JOURNAL OF GUIDANCE, CONTROL, AND DYNAMICS
Vol. 29, No. 6, November–December 2006

# Affine Parameter-Dependent Preview Control for Rotorcraft Terrain Following Flight

Nuno Paulino,* Carlos Silvestre,† and Rita Cunha‡
*Instituto Superior Técnico, Institute for Systems and Robotics, 1049-001 Lisbon, Portugal*

DOI: 10.2514/1.19341

**This paper presents a terrain-following controller for rotorcraft that takes into account the terrain characteristics ahead of the vehicle as measured by a laser range scanner. The methodology used to solve the terrain-following control problem poses it as a discrete time path following control problem in which a conveniently defined error state-space model of the plant is augmented with terrain preview data. A piecewise affine parameter-dependent model representation is used to accurately describe the linearized error dynamics for a predefined set of operating regions. For each region, the synthesis problem is stated as a state feedback $H_2$ control problem for affine parameter-dependent systems and solved using linear matrix inequalities. An alternative technique to compute the feedforward preview gain matrix is proposed that avoids solving linear matrix inequalities involving a large number of unknowns. The resulting nonlinear controller is implemented within the scope of gain-scheduled control theory using the D-methodology. Simulation results obtained with the full nonlinear helicopter model are presented and discussed.**

## I. Introduction

RECENT advances in sensor technology and the increasing availability of computational capacity are steadily affording unmanned air vehicles (UAVs) higher degrees of robustness and reliability in challenging and uncertain operation scenarios. Model-scale helicopters constitute one of the most versatile and cost-effective UAV platforms with a wide and valuable range of applications, such as crop spraying, fire surveillance, and bridge and building inspection. Unlike fixed-wing aircraft, helicopters were designed to execute vertical flight maneuvers, including hovering and vertical takeoff and landing (VTOL). Moreover, their ability to perform agile maneuvers both at high and low speeds does not undermine the good flying qualities displayed in fast forward flight. The tradeoff for such maneuverability is an inherent complexity that translates into a highly nonlinear and unstable dynamical system with wide parameter variations over the vehicle's flight envelope. In this context, the development of terrain-following control systems constitutes both a challenge and a fundamental requirement for accomplishing high performance low altitude autonomous flight.

This paper presents a terrain-following controller, based on a novel preview control algorithm. Preview control algorithms have been widely used to improve the overall closed-loop performance obtained with limited bandwidth feedback compensators when future information on the commands or disturbances is available. A series of papers on application of the linear quadratic preview control theory to the design of vehicle active suspensions can be found in the literature. Special emphasis should be given to the pioneering work of Tomizuka [1], where the optimal preview control problem is formulated and solved, and the impact of different preview lengths on the overall suspension performance is discussed. An alternative method is presented by Prokop and Sharp [2] that consists of incorporating the disturbance or reference dynamics into the design model and then solving the resulting linear quadratic control problem. More recently, Takaba [3] addressed the problem of a robust servomechanism with preview action mixed LQ/$H_\infty$ design for polytopic uncertain systems using Linear Matrix Inequalities.

Related work in the area with applications to helicopters can be found in [4], in which the authors apply the generalized predictive control algorithm to a rotorcraft terrain-following problem. In this work, the performance of the resultant controller is compared with that of a conventional compensator in terms of flight path following, control activity, and control law implementation.

For linear control systems design, the paper exploits the use of a discrete time state feedback $H_2$ preview control problem for affine parameter-dependent systems. Much of the work in this area is well rooted in the theory of linear matrix inequalities (LMIs), which are steadily becoming a standard tool for advanced control system design. In fact, many control problems can be cast as LMI problems that can be solved efficiently using convex programming techniques. In this paper, results presented in [3,5,6] were used to develop the LMI-based $H_2$ preview controller synthesis algorithm for affine parameter-dependent systems. For large preview intervals, the technique proposed in the paper leads to LMI optimization problems involving a large number of variables. To tackle this problem, an alternative algorithm for computing the feedforward gain matrix is proposed, one which exploits the particular structure of the augmented preview system.

In the paper, linear state feedback preview controllers are synthesized for a finite number of piecewise affine parameter-dependent discrete time plant models. Each of these models consists of the discrete equivalent of the generalized error linearization for each of the helicopter operating regions determined by a well-defined box in the parameter space (vehicle's total speed and angle of attack). The adopted error space is in line with the solutions presented in [7–9] and exhibits high directionality accuracy, by taking into account the current vehicle orientation in the definition of the reference velocities.

The resulting controllers are then switched as function of the scheduling variables that parametrize the helicopter operating regions. The final implementation of the nonlinear gain-scheduled controller is obtained using the D-methodology presented in Kaminer et al. [10], which guarantees a fundamental linearization property and avoids the need to feedforward the values of the state variables and inputs at trimming.

A key question underlying the design of sensor based terrain-following control systems is computation of the terrain elevation data from sensor measurements. In this paper, the technique adopted

Presented as Paper 6370 at the AIAA Guidance, Navigation, and Control Conference and Exhibit, San Francisco California, 15–18 August 2005; received 5 August 2005; revision received 8 February 2006; accepted for publication 8 February 2006. 

*M.S. Student, Department of Electrical Engineering and Computer Science, Avenida Rovisco Pais 1; paulino@isr.ist.utl.pt.

†Assistant Professor, Department of Electrical Engineering and Computer Science, Avenida Rovisco Pais 1; cjs@isr.ist.utl.pt. Member AIAA.

‡Ph.D. Student, Department of Electrical Engineering and Computer Science, Avenida Rovisco Pais 1; rita@isr.ist.utl.pt.

exploits the sensor geometry to efficiently build the terrain profile ahead of the vehicle.

The controller design and performance evaluation of the overall closed-loop system relies on an accurate self-contained helicopter dynamic model, derived from first-principles, that is specially tailored for model-scale helicopters [11]. The simulation model, implemented in Matlab, using Simulink and CMEX-file S-functions, includes rigid-body, main rotor flapping, and Bell–Hiller stabilizing bar dynamics and is parametrized for the case of the Vario X-Treme acrobatic helicopter.

The paper is organized as follows. In Sec. II, a nonlinear dynamic model for model-scale helicopters is presented. Section III introduces the path-dependent error space used to describe the vehicle dynamics. Section IV states the preview control problem. Section V describes the methodology adopted for $H_2$ linear controller design where an LMI synthesis technique is applied to affine parameter-dependent systems. Section VI presents the reconstruction technique used to build the reference path from laser range scanner measurements. Section VII focuses on implementation of the nonlinear terrain-following controller for the Vario X-treme helicopter. Finally, simulation results obtained with the full nonlinear dynamic model are presented in Sec. VIII.

## II. Helicopter Dynamic Model

The helicopter dynamic model presented here was the basis for development of a simulator, named SimModHeli [11], implemented in Matlab, using Simulink and C MEX-file S-functions, which is freely available to the scientific community. This simulator is completely parametrizable and describes the dynamics of helicopters with any number of blades, with or without a Hiller or Bell–Hiller stabilizing bar. The simulation model is specially tailored for model-scale helicopters, such as the one depicted in Fig. 1. In this paper, for controller design purposes, a simplified model adequate for low speed flight regimes is adopted. The analysis leading to this simplified model is discussed in Cunha and Silvestre [11].

The helicopter dynamics are described using a conventional 6 degrees of freedom rigid-body model driven by forces and moments that explicitly include the effects of the main rotor, Bell–Hiller stabilizing bar, tail rotor, fuselage, horizontal tailplane, and vertical fin. The main rotor is the primary source of lift and propulsion, generating forces and moments that enable control of the aircraft position, orientation, and velocity. The Bell–Hiller stabilizing bar improves the stability characteristics of the helicopter. The tail rotor, located at the tail boom, provides the moment needed to counteract the torque generated by the aerodynamic drag forces at the rotor hub. The remaining components have less significant contributions and can be described by simpler models. In short, the fuselage produces drag forces and moments and the horizontal tailplane and vertical fin act as wings in forward flight, increasing flight efficiency. A detailed description of the helicopter dynamic model can be found in Cunha and Silvestre [11].

The equations of motion were derived using the following notation:

1) $\{I\}$: inertial coordinate frame;

**Fig. 1** ***Vario X-treme*** **model-scale helicopter.**

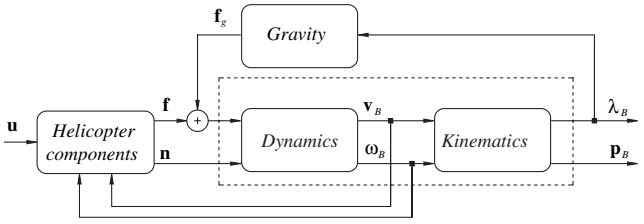


**Fig. 2 Block diagram of the nonlinear model.**

2) $\{B\}$: body-fixed coordinate frame, with origin at the vehicle's center of mass;

3) $\mathbf{p}_B = [x, y, z]^T$: position of the vehicle's center of mass, expressed in $\{I\}$;

4) $\boldsymbol{\lambda}_B = [\phi_B, \theta_B, \psi_B]^T$: $Z$–$Y$–$X$ Euler angles that locally parametrize the orientation of the vehicle relative to $\{I\}$;

5) $\mathbf{v}_B = [u, v, w]^T$: body-fixed linear velocity vector;

6) $\boldsymbol{\omega}_B = [p, q, r]^T$: body-fixed angular velocity vector.

Figure 2 captures the general structure of a rigid-body helicopter model, which can be written as

$$\begin{cases} m\dot{\mathbf{v}}_B = \mathbf{f}(\mathbf{v}_B, \boldsymbol{\omega}_B, \mathbf{u}) + m_I^B \mathcal{R}[0\ 0\ G]^T - \mathcal{S}(\boldsymbol{\omega}_B) m\mathbf{v}_B \\ I_B\dot{\boldsymbol{\omega}}_B = \mathbf{n}(\mathbf{v}_B, \boldsymbol{\omega}_B, \mathbf{u}) - \mathcal{S}(\boldsymbol{\omega}_B) I_B \boldsymbol{\omega}_B \\ \dot{\mathbf{p}}_B = {}_I^B\mathcal{R}\mathbf{v}_B \\ \dot{\boldsymbol{\lambda}}_B = \mathcal{Q}(\phi_B, \theta_B)\boldsymbol{\omega}_B \end{cases} \tag{1}$$

where $m$ is the vehicle's mass, $I_B$ is the inertia about the $\{B\}$ frame, $\mathbf{f}$ and $\mathbf{n}$ are the vectors of external forces and moments, respectively, $g$ is the gravitational acceleration, ${}_I^B\mathcal{R}$ is the rotation matrix from $\{I\}$ to $\{B\}$, $\mathcal{S}(\mathbf{x})$ is a skew-symmetric matrix, defined such that $\mathcal{S}(\mathbf{x})\mathbf{y} = \mathbf{x} \times \mathbf{y}$, and $\mathcal{Q}(\phi_B, \theta_B)$ is the transformation from angular speeds to Euler angle derivatives given by

$$\mathcal{Q}(\phi_B, \theta_B) = \begin{bmatrix} 1 & \sin\phi_B \tan\theta_B & \cos\phi_B \tan\phi_B \\ 0 & \cos\phi_B & -\sin\phi_B \\ 0 & \sin\phi_B/\cos\theta_B & \cos\phi_B/\cos\theta_B \end{bmatrix}$$

The external force and moment vectors are functions of the vehicle velocities and of the command vector $\mathbf{u} = [\theta_0, \theta_{1c}, \theta_{1s}, \theta_{0t}]^T$, which consists of the main rotor collective input $\theta_0$, main rotor and flybar cyclic inputs $\theta_{1c}$ and $\theta_{1s}$, and tail rotor collective input $\theta_{0t}$.

## III. Error Space

The problem of steering the vehicle along a predefined path, which ultimately allows for definition of a terrain-following controller, can be converted into a regulation problem by expressing the state of the vehicle in a conveniently defined error space. This definition requires the introduction of two coordinate systems: the Serret–Frenet frame $\{T\}$ with origin at the point on the path closest to the vehicle and coordinate axes corresponding to the tangent, normal, and binormal vectors defined at that point; and the desired body frame $\{C\}$ which defines the reference for orientation at each point on the path (see Fig. 3). References for the tangent velocities are also required, with $\mathbf{v}_r = [V_r\ 0\ 0]^T$ denoting the desired linear velocity and $\boldsymbol{\omega}_r$ the desired angular velocity.

Given these definitions, and according to [7], an error state vector $\mathbf{x}_e \in \mathbb{R}^{11}$ and output $\mathbf{y}_e \in \mathbb{R}^4$ can be introduced

$$\mathbf{x}_e = \begin{bmatrix} \mathbf{v}_e \\ \boldsymbol{\omega}_e \\ \mathbf{d}_t \\ \boldsymbol{\lambda}_e \end{bmatrix} = \begin{bmatrix} \mathbf{v}_B - {}_T^B\mathcal{R}\mathbf{v}_r \\ \boldsymbol{\omega}_B - {}_T^B\mathcal{R}\boldsymbol{\omega}_r \\ \Pi_{yz}\,{}_I^T\mathcal{R}(\mathbf{p}_B - \mathbf{p}_C) \\ \boldsymbol{\lambda}_B - \boldsymbol{\lambda}_C \end{bmatrix} \tag{2}$$

and

$$\mathbf{y}_e = \begin{bmatrix} \mathbf{v}_e + {}_T^B\mathcal{R}[0\ \mathbf{d}_t^T]^T \\ \psi_e \end{bmatrix} \tag{3}$$

where

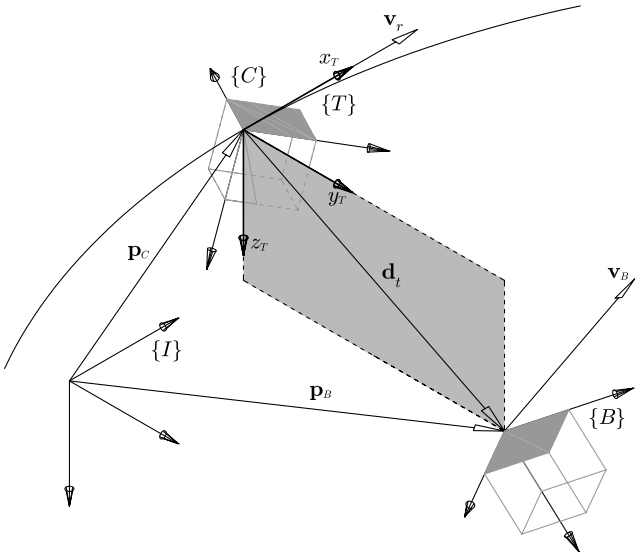


**Fig. 3 Coordinate frames: Inertial $\{I\}$; body $\{B\}$; Serret–Frenet $\{T\}$; desired body $\{C\}$.**

$$\Pi_{yz} = \begin{bmatrix} 0 & 1 & 0 \\ 0 & 0 & 1 \end{bmatrix}$$

the vectors $\mathbf{p}_B$ and $\mathbf{p}_C$ are the origins of $\{B\}$ and $\{C\}$ expressed in $\{I\}$, and $\boldsymbol{\lambda}_C$ is the vector of Euler angles representing the orientation of $\{C\}$ with respect to $\{I\}$. It is straightforward to verify that the vehicle follows the path with tangent velocities $\mathbf{v}_r$ and $\boldsymbol{\omega}_r$ and orientation $\boldsymbol{\lambda}_C$ if and only if $\mathbf{x}_e = 0$.

The output vector $\mathbf{y}_e$ corresponds to a combination of error vector components expressed on the body coordinate system, which is added for tracking purposes. By including $\mathbf{v}_e$ and $\mathbf{d}_t$ in $\mathbf{y}_e$, both the velocity and position errors are being considered, with the distance vector expressed in the current body frame. The choice of $\psi_e$ as the remaining output arises from the specific characteristics of the helicopter. It can be shown that a helicopter may describe a trimming trajectory, with arbitrary but constant yaw angle relative to the path being followed, automatically constraining the roll and pitch angles.

Assuming that the reference path satisfies $\boldsymbol{\omega}_r = 0$, $\dot{\boldsymbol{\lambda}}_C = 0$, the error dynamics can be written as

$$\begin{cases} \dot{\mathbf{v}}_e = \dot{\mathbf{v}}_B + \mathcal{S}(\boldsymbol{\omega}_e){}^B_T\mathcal{R}\mathbf{v}_r - {}^B_I\mathcal{R}(\mathrm{d}/\mathrm{d}t)({}^I_T\mathcal{R}\mathbf{v}_r) \\ \dot{\boldsymbol{\omega}}_e = \dot{\boldsymbol{\omega}}_B \\ \dot{\mathbf{d}}_t = \Pi_{yz}{}^T_B\mathcal{R}\mathbf{v}_e - \Pi_{yz}\mathcal{S}(\boldsymbol{\omega}_T)[0 \;\; \mathbf{d}_t^T]^T \\ \dot{\boldsymbol{\lambda}}_e = \mathcal{Q}(\phi_e + \phi_C, \theta_e + \theta_C)\boldsymbol{\omega}_e \end{cases} \tag{4}$$

where $\boldsymbol{\omega}_T = {}^T_I\mathcal{R}^I\boldsymbol{\omega}_T$ is the angular velocity of $\{T\}$ relative to $\{I\}$ expressed in $\{T\}$. Further details on the derivation of the error dynamics can be found in Cunha and Silvestre [7].

For a given straight line path ($\boldsymbol{\omega}_T = 0$), linear speed $V_r$, and orientation $\boldsymbol{\lambda}_C$, define $\mathbf{u}_c$ as the constant input vector that satisfies (1) at equilibrium ($\dot{\mathbf{v}}_B = 0$, $\dot{\boldsymbol{\omega}}_B = 0$), with $\mathbf{v}_B = {}^C_T\mathcal{R}\mathbf{v}_r$, $\boldsymbol{\omega}_B = 0$, and $\boldsymbol{\lambda}_B = \boldsymbol{\lambda}_C$. Then, the linearization of (4) with output vector $\mathbf{y}_e$ about the equilibrium point $\mathbf{x}_e = 0$, $\mathbf{u} = \mathbf{u}_c$ results in

$$\delta\dot{\mathbf{x}}_e = A_e\delta\mathbf{x}_e + B_e\delta\mathbf{u} \tag{5}$$

$$\delta\mathbf{y}_e = C_e\delta\mathbf{x}_e \tag{6}$$

where $A_e$, $B_e$, and $C_e$ denote the Jacobians evaluated at the equilibrium condition.

The discrete time equivalent of the linear continuous time model (5) is obtained using the zero-order hold on the inputs technique. Let $T$ be the sampling time and define, with obvious abuse of notation, the augmented discrete time state $\mathbf{x}_d(k) = [\mathbf{x}_e(k)^T, \mathbf{x}_i(k)^T]^T$, where $\mathbf{x}_i(k)$ corresponds to the discrete time integral of $\mathbf{y}_e$. Using this notation, the discrete error dynamics can be written as

$$\mathbf{x}_d(k+1) = A\mathbf{x}_d(k) + B\mathbf{u}(k) \tag{7}$$

where

$$A = \begin{bmatrix} e^{A_eT} & 0 \\ C_e & I \end{bmatrix} \quad \text{and} \quad B = \begin{bmatrix} \int_0^T e^{A_e\tau}\,\mathrm{d}\tau B_e \\ 0 \end{bmatrix}$$

## IV. Preview Problem Formulation

Better terrain-following performance with limited bandwidth compensators can be achieved by taking into account, in the control law, the terrain characteristics ahead of the helicopter obtained from measurements of a forward looking laser range scanner. The technique used in this paper to develop a tracking controller generalizes the results presented in Libório et al. [12], and amounts to augmenting the discrete time error space dynamics with a description of the future terrain evolution as seen by the platform.

With the objective of including future path disturbances in the discrete time error space dynamics (7), assume that the helicopter moves with constant speed and attitude along a given reference path that results from the concatenation of straight lines. A detailed analysis of the error dynamics (4) suggests the introduction of the term ${}^I\dot{\mathbf{v}}_r = (\mathrm{d}/\mathrm{d}t)({}^I_T\mathcal{R}\mathbf{v}_r)$ as the perturbation to be previewed. Using this interpretation, the disturbance signal, as seen from the helicopter, can be modeled as ${}^I\dot{\mathbf{v}}_r(t) = \sum_i \mathbf{s}(t_i)\delta(t - t_i)$, where $\mathbf{s}(t_i)$ represents an intensity vector, $\delta(t - t_i)$ is the Dirac's delta function, and $t_i$ corresponds to the $i$th concatenation point crossing time. From (5) the resulting linear error dynamics can be written as

$$\delta\dot{\mathbf{x}}_e = A_e\delta\mathbf{x}_e + B_e\delta\mathbf{u} + W\delta{}^I\dot{\mathbf{v}}_r, \qquad W = \begin{bmatrix} -{}^C_I\mathcal{R}^T & 0 \end{bmatrix}^T \tag{8}$$

and the corresponding discretization is given by

$$\mathbf{x}_d(k+1) = A\mathbf{x}_d(k) + B\mathbf{u}(k) + B_1\mathbf{s}(k) \tag{9}$$

where $B_1 = [(e^{A_eT}W)^T, 0]^T$ is obtained from the impulse invariant discrete equivalent of the injection matrix $W$. It is assumed that the sampling period is sufficiently small to consider the reference path changes synchronized with the sampling time. Once again with obvious abuse of notation, $\mathbf{s}(k) \in \mathbb{R}^s$ corresponds to

$$\mathbf{s}(k) = {}^I\mathbf{v}_r(k+1) - {}^I\mathbf{v}_r(k) \tag{10}$$

Assuming a preview length of $p$ samples, let $\mathbf{x}_s(k) = [\mathbf{s}(k)^T, \mathbf{s}(k+1)^T, \ldots, \mathbf{s}(k+p)^T]^T \in \mathbb{R}^{[s(p+1)]\times 1}$ be the vector containing all the preview inputs at instant $k$. The discrete time dynamics of vector $\mathbf{x}_s(k)$ can be modeled as a FIFO queue, given by

$$\mathbf{x}_s(k+1) = D\mathbf{x}_s(k) + B_s\mathbf{s}(k+p+1) \tag{11}$$

where

$$D = \begin{bmatrix} 0 & I & 0 & \cdots & 0 \\ 0 & 0 & I & \cdots & 0 \\ \vdots & \vdots & \ddots & \ddots & \vdots \\ 0 & 0 & 0 & \ddots & I \\ 0 & 0 & 0 & \cdots & 0 \end{bmatrix}, \qquad B_s = \begin{bmatrix} 0 \\ 0 \\ \vdots \\ I \end{bmatrix}$$

Combining the dynamic representation of the terrain (11) with (9) yields the augmented system

$$\mathbf{x}(k+1) = \bar{A}\mathbf{x}(k) + \bar{B}_s\mathbf{s}(k) + \bar{B}\mathbf{u}(k) \tag{12}$$

where

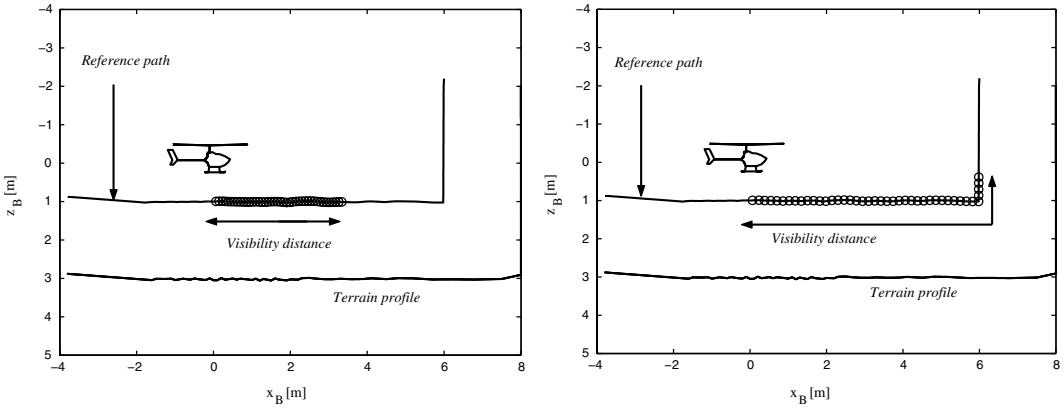


**a)** $V_t = 4\,\mathrm{ms}^{-1}$ **b)** $V_t = 8\,\mathrm{ms}^{-1}$

**Fig. 4 Representation of 40 preview samples over the reference path for different speeds.**

$$\mathbf{x}(k) = \begin{bmatrix} \mathbf{x}_d(k) \\ \mathbf{x}_s(k) \end{bmatrix}, \qquad \bar{A} = \begin{bmatrix} A & H \\ 0 & D \end{bmatrix}$$

$$\bar{B}_s = \begin{bmatrix} 0 \\ B_s \end{bmatrix}, \qquad \bar{B} = \begin{bmatrix} B \\ 0 \end{bmatrix}$$

and $H = [B_1, 0, 0, \ldots, 0]$ represents the injection matrix of the preview signals into the error dynamics. Notice that the $D$ matrix is stable and therefore the augmented system (12) preserves the stabilizability and detectability properties of the original plant.

With the present technique, the preview information is retrieved at $p$ points selected along the path, equally spaced by the distance $d_p = V_t(k)T$. The scalar $V_t(k)$ corresponds to the norm of the projection of the vehicle's velocity vector $\mathbf{v}_B$ on the path, computed at instant $k$, which can be obtained from $V_t = [1\ 0\ 0]_B^T \mathcal{R}\mathbf{v}_B$. This fact turns out to be of utmost importance, because it allows one to naturally redefine the controller visibility distance as a function of the vehicle's speed, preserving the size of the preview input vector. An example of this property is shown in Fig. 4, in which path preview vectors were obtained for two different speeds. From the figure, it becomes clear how the vehicle velocity has an impact on the visibility distance. The limit case $\mathbf{v}_B \to 0$ results in a pure hovering maneuver where the preview samples are taken from a fixed point on the path.

## V. Discrete Time Controller Design

This section presents a solution for the discrete time state feedback $H_2$ preview control problem for affine parameter-dependent systems. In the approach pursued in this paper, results presented in [3,5,6] were used to develop the LMI-based controller synthesis algorithm. Much of the work in this area is well rooted in the theory of LMIs, which are steadily becoming a standard tool for advanced control system design. In fact, LMIs provide a powerful formulation framework as well as a versatile design technique for a wide variety of linear control problems. Because solving LMIs is a convex optimization problem for which numerical solvers are now available, an LMI-based formulation can be seen as a practical solution for many control problems.

### A. Theoretical Background

In what follows, the standard setup and nomenclature used in [13] is adopted, leading to the state-space LFT feedback system represented in Fig. 5. Consider the generalized affine parameter-dependent system $\mathbf{G}(\boldsymbol{\zeta})$ as a function of the slowly varying parameter vector $\boldsymbol{\zeta}$. It is assumed that $\boldsymbol{\zeta}$ is in a compact set $\Theta \in \mathbb{R}^q$. Suppose that the parameter set $\Theta$ can be partitioned into a family of regions that are compact closed subsets $\Theta_i$, $i = 1, \ldots, N$ and that cover the desired helicopter flight envelope. In the $i$th parameter region $\boldsymbol{\zeta} \in \Theta_i$ the dynamic behavior of the closed-loop system satisfies the realization

$$\begin{cases} \mathbf{x}(k+1) = A(\boldsymbol{\zeta})\mathbf{x}(k) + B_w(\boldsymbol{\zeta})\mathbf{w}(k) + B(\boldsymbol{\zeta})\mathbf{u}(k), \\ \mathbf{z}(k) = C_z(\boldsymbol{\zeta})\mathbf{x}(k) + E(\boldsymbol{\zeta})\mathbf{u}(k), \end{cases}$$

$$\mathbf{u}(k) = K\mathbf{x}(k) \qquad (13)$$

where $\mathbf{x}(k)$ is the state vector. The symbol $\mathbf{w}(k)$ denotes the input vector of exogenous signals (including commands, disturbances, and preview signals), $\mathbf{z}(k)$ is the output vector of errors to be reduced during the controller design process, and $\mathbf{u}(k)$ is the vector of actuation signals. Matrices $A(\boldsymbol{\zeta})$, $B_w(\boldsymbol{\zeta})$, $B(\boldsymbol{\zeta})$, $C_z(\boldsymbol{\zeta})$, and $E(\boldsymbol{\zeta})$ are affine functions of the parameter vector $\boldsymbol{\zeta} = [\zeta_1, \ldots, \zeta_q]^T$, for example, $A(\boldsymbol{\zeta}) = A^{(0)} + \zeta_1 A^{(1)} + \ldots + \zeta_q A^{(q)}$. The generalized affine parameter-dependent system $G(\boldsymbol{\zeta})$ consists of the plant to be controlled, together with appended weights that shape the exogenous and internal signals and the preview dynamics presented in Sec. IV.

For a given parameter region $\Delta \equiv \Theta_i$, assume that the elements that constitute the parameter vector $\boldsymbol{\zeta}$ have their values confined to the interval $\zeta_j \in [\underline{\zeta}_j, \bar{\zeta}_j]$, $\bar{\zeta}_j \geq \underline{\zeta}_j$, $j = 1, \ldots, q$ and define $\Delta_0$ as the set of the $m = 2^q$ vertices of the parameter-dependent region

$$\Delta_0 := \{\boldsymbol{\zeta} = [\zeta_1, \ldots, \zeta_q]^T : \zeta_j \in \{\underline{\zeta}_j, \bar{\zeta}_j\}, j = 1, \ldots, q\}$$

Then $\Delta$ corresponds to the convex hull of $\Delta_0$, $\Delta = \mathrm{co}\{\Delta_0\}$, which is the smallest convex set containing all the points in $\Delta_0$. The following result, which can be found in [5], is fundamental for affine parameter-dependent systems.

*Result 1*: Let $f : \Delta \to \mathbb{R}$ be a convex function where $\Delta = \mathrm{co}\{\Delta_0\}$. Then $f(\boldsymbol{\zeta}) \leq \gamma$, $\forall\ \boldsymbol{\zeta} \in \Delta$, if an only if $f(\boldsymbol{\zeta}) \leq \gamma$, $\forall\ \boldsymbol{\zeta} \in \Delta_0$.

Suppose that the feedback system is well posed, and let $T_{\mathbf{zw}}$ denote the closed-loop operator from $\mathbf{w}$ to $\mathbf{z}$. The discrete time state feedback $H_2$ synthesis problem consists of finding (if it exists) a static controller $K$ that stabilizes the closed-loop system and makes the $H_2$ norm $\|T_{\mathbf{zw}}\|_2$ of the operator $T_{\mathbf{zw}}$ smaller than a desired bound $\gamma > 0$. The technique used for controller design relies on results available in [5,14], the most important of which are summarized below after being rewritten for the case of affine parameter-dependent systems.

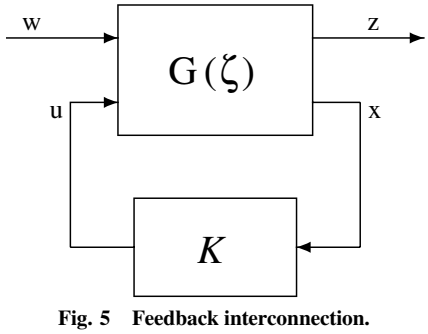


**Fig. 5 Feedback interconnection.**

In the following, tr$(L)$, im$(L)$, and ker$(L)$ denote the trace, image, and kernel of matrix $L$, respectively, and $A_i$, $B_i$, $C_{z_i}$, $E_i$, and $B_{w_i}$ represent the state-space matrices of (13) for the $i = 1, \ldots, m$ points in $\Delta_0$.

*Result 2*: A static state feedback controller guarantees the $\gamma$ upper-bound for the discrete time $H_2$ norm of the closed-loop operator $T_{\mathbf{zw}}(\boldsymbol{\zeta})$ with $\boldsymbol{\zeta} \in \Delta$, that is

$$\|T_{\mathrm{zw}}(\boldsymbol{\zeta})\|_2 = \|(C_z(\boldsymbol{\zeta}) + E(\boldsymbol{\zeta})K)(zI - A(\boldsymbol{\zeta}) - B(\boldsymbol{\zeta})K)^{-1}B_w(\boldsymbol{\zeta})\|_2 < \gamma, \quad \forall\ \boldsymbol{\zeta} \in \Delta \tag{14}$$

if and only if there are real matrices $P = P^T > 0$, $K$ and $Z$ such that the following LMI system is satisfied:

$$\begin{bmatrix} -P^{-1} & (A_i + B_iK) & 0 \\ (A_i + B_iK)^T & -P & (C_{z_i} + E_iK)^T \\ 0 & (C_{z_i} + E_iK) & -I \end{bmatrix} < 0 \tag{15}$$

$$\begin{bmatrix} P^{-1} & B_{w_i} \\ B_{w_i}^T & Z \end{bmatrix} > 0 \tag{16}$$

$$\mathrm{tr}\,(Z) < \gamma^2 \tag{17}$$

It is important to point out that this analysis result states that, to guarantee that matrix $K$ satisfies (14) for all $\boldsymbol{\zeta} \in \Delta$, it is enough to ascertain that $K$ satisfies (14) on the $m$ points of the set $\Delta_0$. The synthesis problem, that is, that of finding a matrix $P = X^{-1}$ and controller $K$ that verify (15–17), can be solved according to the following result:

*Result 3*:The $H_2$ norm of the closed-loop operator $T_{\mathrm{zw}}(\boldsymbol{\zeta})$ is less than a positive number $\gamma$, that is, $\|T_{\mathrm{zw}}\|_2 < \gamma$, with $\boldsymbol{\zeta} \in \Delta$ if a real symmetric matrix $X > 0\,(X = P^{-1})$ and a real matrix $Z$ exist such that

$$(W_{1_i}^T A_i + W_{2_i}^T C_{z_i})X(W_{1_i}^T A_i + W_{2_i}^T C_{z_i})^T - W_{1_i}^T X W_{1_i} - W_{2_i}^T W_{2_i} < 0 \tag{18}$$

$$\begin{bmatrix} X & B_{w_i} \\ B_{w_i}^T & Z \end{bmatrix} > 0 \tag{19}$$

$$\mathrm{tr}\,(Z) < \gamma^2 \tag{20}$$

where matrices $W_{1_i}^T$ and $W_{2_i}^T$ satisfy $\mathrm{im}[W_{1_i}^T\ W_{2_i}^T]^T = \ker[B_i^T\ E_i^T]$. Using the matrix solution $X$, the static state feedback gain $K$ is then computed by solving the following LMI feasibility problem:

$$\begin{bmatrix} -X & A_i & 0 \\ A_i^T & -X^{-1} & C_{z_i}^T \\ 0 & C_{z_i} & -I \end{bmatrix} + \begin{bmatrix} B_i \\ 0 \\ E_i \end{bmatrix} K[0\ I\ 0] + \begin{bmatrix} 0 \\ I \\ 0 \end{bmatrix} K^T[B_i^T\ 0\ E_i^T] < 0 \tag{21}$$

This result can be easily proven by using the projection lemma [5], followed by a decomposition of the null space matrices. Finally, the optimal solution for the discrete time $H_2$ control problem is approximated through the minimization of $\gamma$ subject to Result 3.

### B. Preview Controller Synthesis Technique

For augmented discrete time dynamic systems that include large preview intervals $p > 50$, the controller synthesis technique proposed in the last section leads to LMI optimization problems involving a large number of variables, which cannot easily be solved using the tools available today.

Going back to the preview control problem, consider the linear discrete time system (12). It is well known from the literature [1,2,12] that solutions for $H_2$ discrete time preview control problems can, in general, be decomposed into feedback and feedforward controllers by exploiting the particular structure of augmented preview dynamics. Building on these ideas, an alternative algorithm for computing the feedforward gain matrix is proposed.

To start with, consider an affine parameter-dependent system with the structure of (12), defined over a region $\Delta$, with its $m$ vertices in $\Delta_0$. Restricting the parameter dependency to the state equation, let $\bar{A}_i$, $\bar{B}_i$, $\bar{B}_{w_i}$, $\bar{C}_z$, and $\bar{E}$ denote the state-space matrices for the $i = 1, \ldots, m$ points in $\Delta_0$. Assuming that $\mathbf{s}$ belongs to the disturbance vector $\mathbf{w}$, matrix $\bar{B}_{w_i}$ includes the preview input matrix $\bar{B}_s$. Consider also the central point of $\Delta$, $\boldsymbol{\zeta}_o$, and the corresponding state-space matrices $\bar{A}_o$, $\bar{B}_o$, and $\bar{B}_{w_o}$.

Partitioning matrices according to the augmented system structure, let

$$P = \begin{bmatrix} P_d & P_{ds} \\ P_{ds}^T & P_s \end{bmatrix}$$

$$Q = \bar{C}_z^T\bar{C}_z = \begin{bmatrix} Q_d & Q_{ds} \\ Q_{ds}^T & Q_s \end{bmatrix}$$

$R = \bar{E}^T\bar{E}$, and $K = [K_d, K_s]$. Further assume that $\bar{C}_z^T\bar{E} = 0$. Applying Schur complements to the LMI (15), the following Lyapunov inequality is obtained:

$$(\bar{A}_i + \bar{B}_iK)^T P(\bar{A}_i + \bar{B}_iK) - P + (\bar{C}_z + \bar{E}K)^T(\bar{C}_z + \bar{E}K) < 0 \tag{22}$$

Simple manipulations show that the upper right block of (22) corresponds to a Lyapunov inequality of the form

$$(A_i + B_iK_d)^T P_d(A_i + B_iK_d) - P_d + Q_d + K_d^T R K_d < 0 \tag{23}$$

In view of these facts, the following result can be established.

*Theorem 1*. Given a pair $(P_d, K_d)$, $P_d = P_d^T > 0$ that satisfies the conditions of Results 2, consider the matrix

$$P_{ds} = [\tilde{A}_c^T P_d B_o, (\tilde{A}_c^2)^T P_d B_o, \ldots, (\tilde{A}_c^{p+1})^T P_d B_o] + \left[Q_1, \tilde{A}_c^T Q_1 + Q_2, \ldots, \sum_{j=1}^{p+1}(\tilde{A}_c^{p+1-j})^T Q_j\right] \tag{24}$$

where $\tilde{A}_c = A_o - B_o(B_o^T P_d B_o + R)^{-1}B_o^T P_d A_o$ and $Q_j$ denotes the $j$th $s$-dimensional column block of matrix $Q_{ds}$, and the matrix $P_s$ with entries

$$P_s(i,j) = \begin{cases} \Xi(i,j) & , i \le s \vee j \le s \\ \Xi(i,j) + P_s(i-s, j-s) & , i > s \wedge j > s \end{cases} \tag{25}$$

$$\Xi = H_o^T P_d H_o + H_o^T P_{ds} D + D^T P_{ds} H_o + Q_s - (P_d H_o + P_{ds} D)^T B_o(B_o^T P_d B_o + R)^{-1} B_o^T (P_d H_o + P_{ds} D)$$

Consider also the feedforward gain matrix

$$K_s = (B_o^T P_d B_o + R)^{-1} B_o^T (P_d H_o + P_{ds} D) \tag{26}$$

Then, the resulting closed-loop system is stable over the whole region $\Delta$ and the Lyapunov inequality for the central point verifies

$$(\bar{A}_o + \bar{B}_oK)^T P(\bar{A}_o + \bar{B}_oK) - P + (\bar{C}_z + \bar{E}K)^T(\bar{C}_z + \bar{E}K) = \begin{bmatrix} \Lambda & 0 \\ 0 & 0 \end{bmatrix} \le 0 \tag{27}$$

with $P = P^T > 0$.

*Proof*. Let $K = [K_d, K_s]$ be a stabilizing state feedback controller for system (12). Simple inspection of the structure of (12) shows that only $K_d$ determines the stability of the closed-loop system. Because the pair $(P_d, K_d)$ satisfies the conditions of Result 2 the stability of the closed-loop system over the whole region $\Delta$ is guaranteed.

To show that (27) is verified for the central point, consider the following expressions:

$$L(P,K) \equiv (\bar{A}_o + \bar{B}_o K)^T P(\bar{A}_o + \bar{B}_o K) - P + (\bar{C}_z + \bar{E}K)^T(\bar{C}_z + \bar{E}K)$$

and

$$\tilde{L}(P) \equiv \bar{A}_o^T P \bar{A}_o - P - \bar{A}_o^T P^T \bar{B}_o(\bar{B}_o^T P \bar{B}_o + R)^{-1}\bar{B}_o^T P \bar{A}_o + Q$$

such that $L(P,K) = 0$ and $\tilde{L}(P) = 0$ corresponding to a Lyapunov equation and an algebraic Riccati equation (ARE), respectively. Assuming that $Q = \bar{C}_z^T \bar{C}_z$, $R = \bar{E}^T \bar{E}$, and $\bar{C}_z^T \bar{E} = 0$, it is straightforward to show that

$$L(P,K) = \tilde{L}(P) + (K - \tilde{K})^T(\bar{B}_o^T P \bar{B}_o + R)(K - \tilde{K}) \tag{28}$$

where $\tilde{K} = -(\bar{B}_o^T P \bar{B}_o + R)^{-1}\bar{B}_o^T P \bar{A}_o$. Using the structure of the augmented system matrices, (28) can be written as

$$\begin{bmatrix} \Lambda(P_d,K_d) & \Sigma(P,K) \\ \Sigma(P,K)^T & \Gamma(P,K) \end{bmatrix} = \begin{bmatrix} \tilde{\Lambda}(P_d) & \tilde{\Sigma}(P) \\ \tilde{\Sigma}(P)^T & \tilde{\Gamma}(P) \end{bmatrix} + \begin{bmatrix} K_d^T & \tilde{K}_d^T \\ K_s^T & -\tilde{K}_s^T \end{bmatrix}(\bar{B}_o^T P \bar{B}_o + R)[K_d - \tilde{K}_d, K_s - \tilde{K}_s] \tag{29}$$

where $\Lambda(P_d,K_d) < 0$ corresponds to the Lyapunov inequality (23) and $\tilde{\Lambda}(P_d) = 0$ takes the form of an ARE, both computed for the central system. Because $K_s$ does not influence the stability of the closed-loop system, one can impose that $K_s = \tilde{K}_s = (B_o^T P_d B_o + R)^{-1}B_o^T(P_d H_o + P_{ds} D)$, yielding $\Gamma = \tilde{\Gamma}$ and $\Sigma = \tilde{\Sigma}$.

From the hypothesis, it follows that $\Lambda(P_d,K_d) < 0$, which can be rewritten as $\tilde{\Lambda}(P_d) + (K_d - \tilde{K}_d)^T(B_o^T P_d B_o + R)(K_d - \tilde{K}_d) < 0$, and therefore $\tilde{\Lambda}(P_d) < 0$. Then, there exists a positive definite matrix $\delta Q_d$ such that $P_d$ is the unique positive definite solution to the ARE $\tilde{\Lambda}(P_d) + \delta Q_d = 0$. Defining a new ARE for the augmented system

$$\begin{bmatrix} \tilde{\Lambda}(P) + \delta Q_d & \tilde{\Sigma}(P) \\ \tilde{\Sigma}(P)^T & \tilde{\Gamma}(P) \end{bmatrix} = 0$$

it can be shown that its unique positive definite solution is given by

$$P = \begin{bmatrix} P_d & P_{ds} \\ P_{ds}^T & P_s \end{bmatrix}$$

where $P_{ds}$ and $P_s$ satisfy Eqs. (24) and (25), respectively. □

To evaluate the efficiency and validity of the method proposed for controller synthesis, a comparative analysis of the available methods was carried out. The results, presented in Table 1, include both the computation time and the closed-loop system's $H_2$ norm achieved by using the proposed method and by solving the set of LMI's for the augmented system. The results were computed for a forward flight trimming condition (linear body speed $V = 0.9$ ms$^{-1}$, zero angle of attack) and an increasing number of preview samples. Data presented in the table were obtained with a 3.00 GHz Intel Pentium 4 with 512 MB of RAM running Matlab 6.5.0 on Microsoft Windows XP Professional.

The proposed method is indeed much faster than solving the LMI's for the augmented system, especially as the dimension of the preview vector increases, and achieves $H_2$ norm values very close to the ones given by the LMI optimization. Notice that, in practical terms, computation time for the optimal LMI-based method is no longer acceptable when the number of preview samples reaches 15.

**Table 1 Comparison of computation time and $H_2$ norms**

| | Proposed method | | LMI-based method | |
|---|---|---|---|---|
| $p$ | $\|.\|_2$ | time [s] | $\|.\|_2$ | time [s] |
| 1 | 3.639 | 14.8 | 3.639 | 30.5 |
| 2 | 3.484 | 14.7 | 3.484 | 61.8 |
| 3 | 3.340 | 14.7 | 3.341 | 100.6 |
| 4 | 3.203 | 14.6 | 3.205 | 194.8 |
| 5 | 3.073 | 14.8 | 3.075 | 314.7 |
| 6 | 2.948 | 14.6 | 2.950 | 546.0 |
| 7 | 2.828 | 14.6 | 2.831 | 281.2 |
| 8 | 2.714 | 14.7 | 2.717 | 1312.6 |
| 9 | 2.605 | 14.7 | 2.609 | 1998.1 |
| 10 | 2.503 | 14.7 | 2.507 | 2810.1 |
| 15 | 2.090 | 14.7 | ?[a] | >3600 |
| 20 | 1.845 | 14.7 | ?[a] | >3600 |
| 30 | 1.692 | 14.9 | ?[a] | >3600 |
| 40 | 1.682 | 14.8 | ?[a] | >3600 |
| 50 | 1.677 | 14.9 | ?[a] | >3600 |
| 70 | 1.669 | 15.3 | ?[a] | >3600 |
| 100 | 1.668 | 16.3 | ?[a] | >3600 |

[a]Computation interrupted after 1 h.

## VI. Reference Path

The preview-based tracking controller presented in the previous sections can be applied to terrain following for autonomous helicopters using different range sensing techniques. In this paper, a setup is considered wherein a Laser Range Scanner, mounted underneath the helicopter, scans the terrain along the vehicle's direction of forward flight, see Fig. 8. As a result of this setup, a vector of reference points is available at all times and the full preview vector $\mathbf{x}_s(k)$ can be computed for every sampling instant. To consider this state vector in the tracking controller, it is assumed that for two consecutive sampling instants, the computed reference paths are very similar, so that the dynamics of $\mathbf{x}_s(k)$ can be approximated by (11).

The method adopted to build the reference path from measurement data is now presented. As shown in Fig. 6, the laser readings, consisting of scanning angle and measured range, are transformed into 2-D terrain points, expressed in the body-fixed frame $\{B\}$. All the ensuing processing is performed with respect to this coordinate frame. The reconstruction points are interpolated by straight lines to approximate the terrain profile, whereas the actual reference path is obtained by "rolling" a circle along the reconstructed terrain profile and selecting the maximum for each $x$ coordinate (see Fig. 7). In this way, the reference path is guaranteed to keep a prespecified safety distance from the terrain, defined as a perpendicular offset $D_{\text{off}}$ to the reconstructed terrain profile.

As an example of the path building process, consider the case represented in Fig. 8. It is clear that, for high enough values of the scanning angle, the laser beam no longer hits any obstacle. For these readings, the laser is considered blind and a vertical wall shaped obstacle is assumed, for reasons of simplicity.

The path building algorithm also handles occlusion problems, such as the one depicted in Fig. 9, where the vehicle describes a climbing flight maneuver parallel to the wall and the sensor cannot acquire future information about the terrain profile ahead of this wall. In this specific example, instead of ignoring the two laser readings that do not reach any obstacle, the algorithm uses them to capture the sudden change in the terrain and provide relevant preview information to the control system.

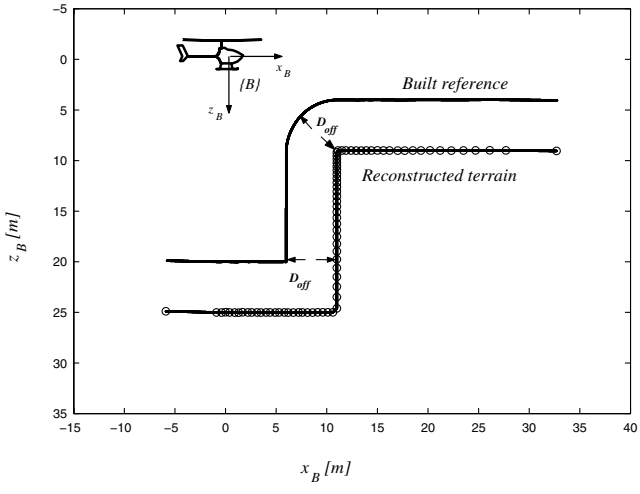


**Fig. 6 Reconstructed terrain profile and corresponding reference path.**

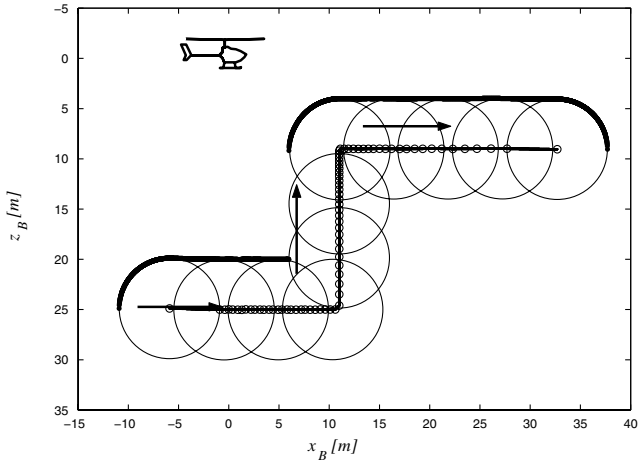


**Fig. 7 Rolling a circle of radius $D_{\text{off}}$, along the terrain profile.**

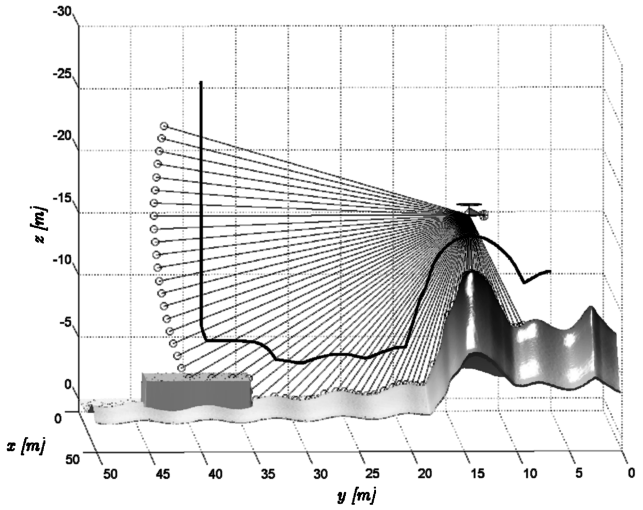


**Fig. 8 Example of terrain profile and corresponding reference path built from laser scan measurements.**

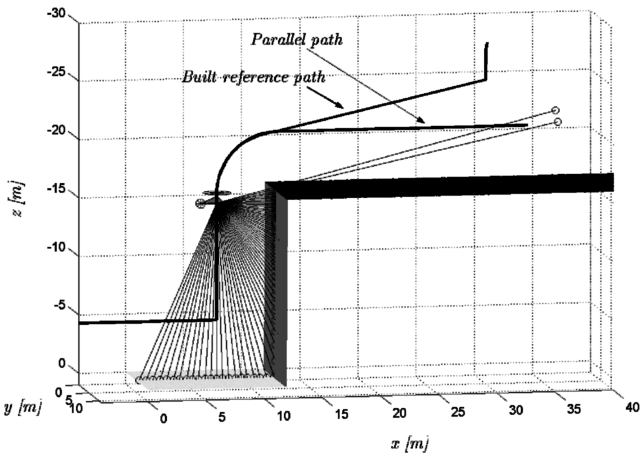


**Fig. 9 Step-shaped terrain and actual reference path computed using out-of-range laser readings.**

## VII. Nonlinear Implementation

In the application presented here the vehicle is expected to follow the terrain moving along a vertical plane, with no sideslip, $\mathbf{v}_B = [u \;\; 0 \;\; w]^T$. Under these assumptions, the angle of attack $\alpha$ and linear body speed $V = \|\mathbf{v}_B\|$ can be, respectively, approximated by $\alpha = \arctan(\frac{w}{u})$, and $V = \sqrt{u^2 + w^2}$. During the controller design phase, the considered helicopter flight envelope was parametrized by $\boldsymbol{\zeta} = [V, \alpha]^T$ and partitioned into the 18 regions presented in Fig. 10.

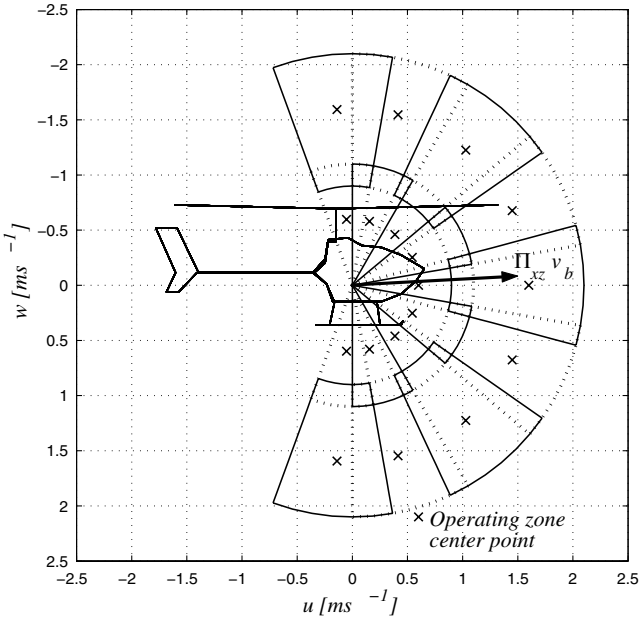


**Fig. 10 Operating regions parametrized by $\boldsymbol{\zeta} = [V, \alpha]^T$ and plotted in the velocity axes $uOw$.**

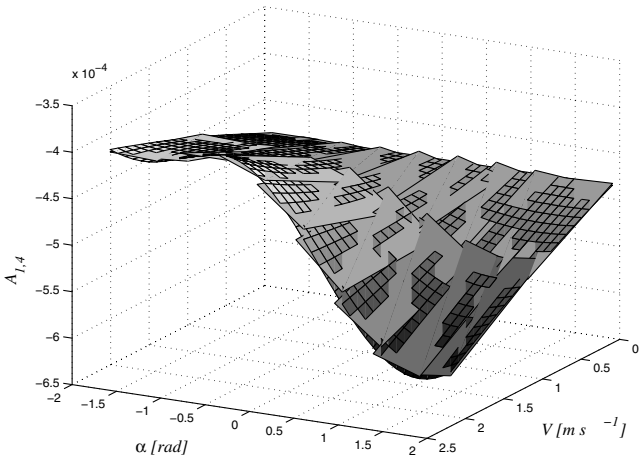


**Fig. 11 Surface and respective affine approximation obtained for element $A_{14}$ as function of the velocity $V$ and angle of attack $\alpha$.**

For each operating region, the elements of the discrete time state-space matrices obtained from linearization of the error dynamics were approximated by affine functions of $\boldsymbol{\zeta}$ using a least squares fitting. As an example, Fig. 11 shows the surface obtained for element (1,4) of matrix $\bar{A}$ and the planes computed for the considered set of operating regions.

For a relatively dense grid of evaluated operating points, the affine approximation results in a maximum absolute error between matrix entries of less than 10% and a average absolute error of less than 2%.

To further validate the affine parameter-dependent approximation, Figs. 12 and 13 display the dominant open-loop eigenvalues for the linearized systems and for the resulting affine approximations. It is important to stress that the eigenvalues have a similar variation with $(V, \alpha)$ and that the number of unstable eigenvalues remains constant.

### A. Controller Implementation

To implement the controller within the scope of gain-scheduling control theory [15], a state feedback matrix gain $K_i$ was computed for each of the operating regions according to the technique presented in Sec. V. During the controller design phase, the regions were defined

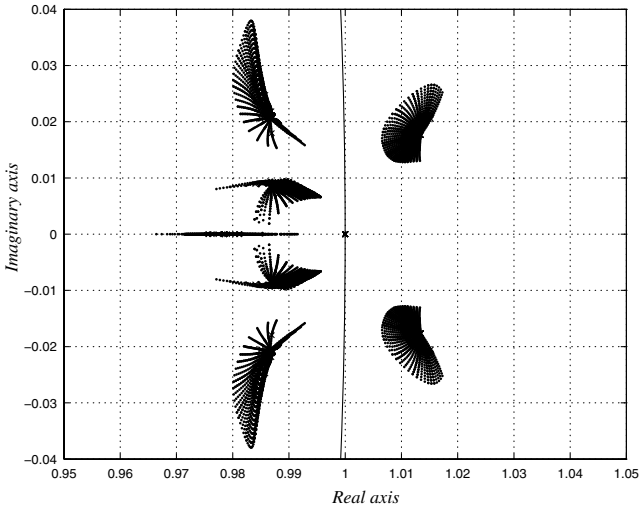


**Fig. 12 Dominant open-loop eigenvalues for the linearized systems.**

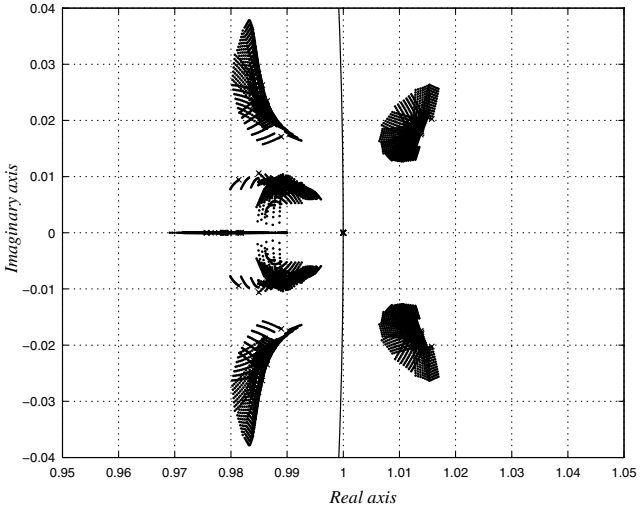


**Fig. 13 Dominant open-loop eigenvalues for the affine approximations.**

as overlaid to avoid fast switching between controllers, see Fig. 10. The disturbance input matrix $\bar{B}_w$ was set to $\bar{B}_s$ and the state and control weight matrices $\bar{C}_z$ and $\bar{E}$ were set to

$$\bar{C}_z = \begin{bmatrix} \mathrm{diag}(\mathbf{c}_z) & \mathbf{0}_{15\times 3(p+1)} \\ \mathbf{0}_{4\times 15} & \mathbf{0}_{4\times 3(p+1)} \end{bmatrix}, \qquad \bar{E} = \begin{bmatrix} \mathbf{0}_{15\times 4} \\ 5I_{4\times 4} \end{bmatrix} \tag{30}$$

where

$$\mathbf{c}_z = [0.5, 0.5, 0.5, 0.1, 0.1, 0.1, 1, 1, 0.01, 0.01, 0.1, 0.1, 0.1, 0.1, 0.1]^T$$

yielding the performance vector

$$\mathbf{z} = [0.5\mathbf{v}_e^T, 0.1\boldsymbol{\omega}_e^T, \mathbf{d}_t^T, 0.01\phi_e, 0.01\theta_e, 0.1\psi_e, 0.1\mathbf{x}_i^T, 5.0\mathbf{u}^T]^T \tag{31}$$

The final implementation scheme, presented in Fig. 14, was achieved using the D-methodology described in Kaminer [10]. This methodology moves all integrators to the plant input, and adds differentiators where they are needed to preserve the transfer functions and the stability characteristics of the closed-loop system. The D-methodology implementation has several important features that are worth emphasizing: 1) autotrimming property—the controller automatically generates adequate trimming values for the actuation signals and for the state variables that are not required to track reference inputs; 2) the implementation of antiwindup schemes

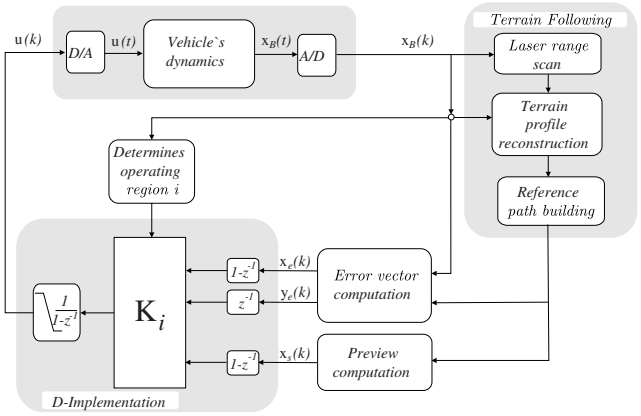


**Fig. 14 Implementation setup using gain scheduling and the D methodology.**

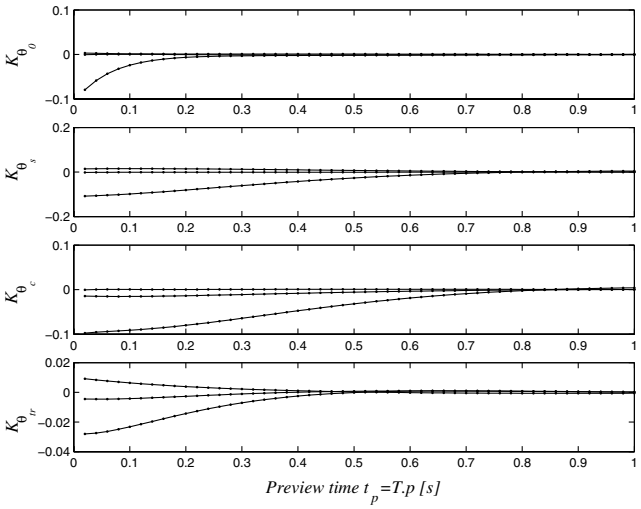


**Fig. 15 Evolution of the preview gains as a function of preview time.**

is straightforward, due to the placement of the integrators at the plant input.

## VIII. Results

The following simulation results were obtained using the nonlinear dynamic model *SimModHeli*, which includes not only the rigid-body dynamics but also the main rotor and Bell–Hiller stabilizing bar flapping dynamics. The model was parametrized for the Vario X-treme platform.

Figure 15 presents the entries of the preview feedforward control matrix $K_s$ as a function of the preview time. In this case, a preview interval of 1 s, sampled at $T = 0.02$ s, is considered. It is clear that the weight of the preview signal decreases as the corresponding instant of time gets further ahead in the future, with negligible contributions above 0.8 s of preview time.

An additional tool used to assess the performance of the preview control scheme consists of comparing the $H_2$ norm of the linear closed-loop systems resulting from application of the control strategies with and without preview action. As shown in Fig. 16, considering a mesh of operating points defined in $V$ and $\alpha$, the performance index for the preview-based solution is consistently below that of the traditional solution.

In Fig. 17, the terrain-following performance obtained with the proposed scheme is evaluated by varying the size of the preview vector and comparing the trajectories described by the vehicle, while following a step-shaped terrain profile. It can be observed that increasing the number of preview samples, up to the value of 30, produces a clear improvement in performance. The fact that after a certain threshold no significant improvement is achieved is a natural

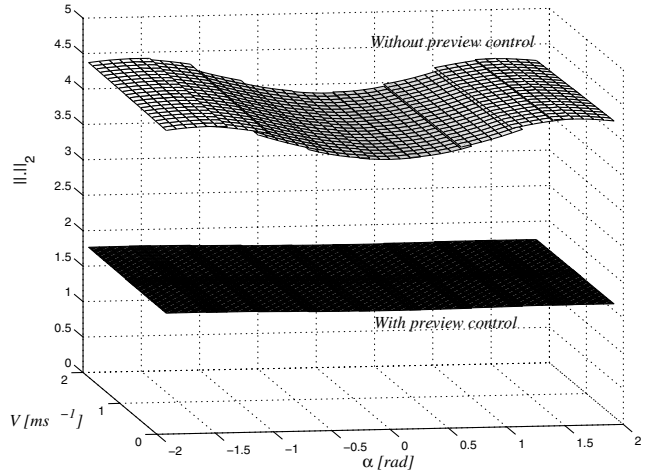


**Fig. 16 Closed-loop system's $H_2$ norm obtained with and without preview.**

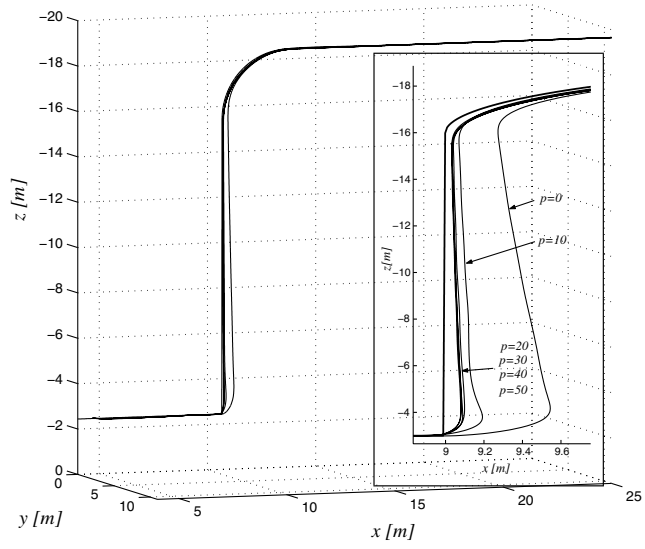


**Fig. 17 Terrain-following performance obtained for different values of $p$, the size of the preview vector.**

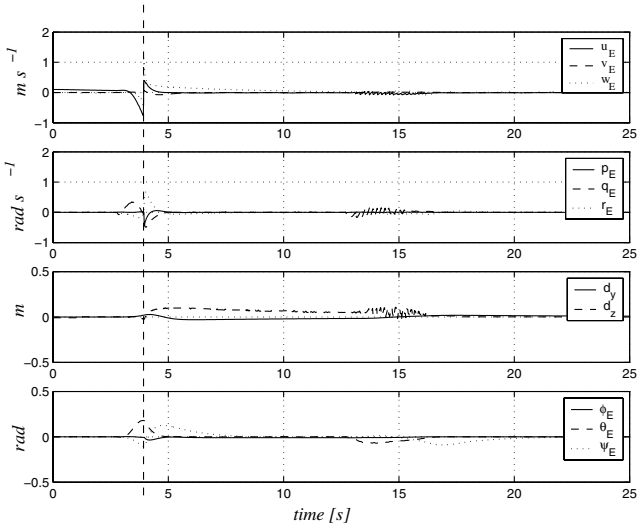


**Fig. 18 Time evolution of the error state $\mathbf{x}_e$.**

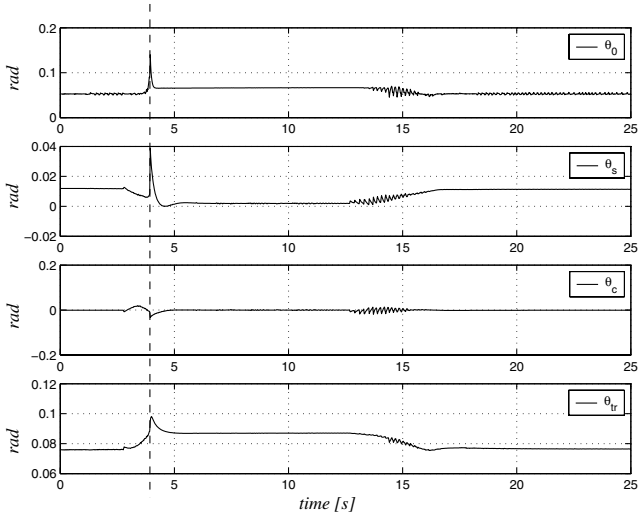


**Fig. 19 Time evolution of the actuation $\mathbf{u}$.**

result and corroborates the expected properties of the proposed method.

The time evolution of the error state vector $\mathbf{x}_e$ and actuation signals $\mathbf{u}$ corresponding to the $p = 50$ experiment is presented in Figs. 18 and 19, respectively. It can be observed that signal activity, due to the preview action, clearly precedes transition points in the reference path. The vertical line marks the change in the reference path from forward to vertical flight. After each transition, both the state and input quickly converge to trimming values.

## IX. Conclusions

The paper presented the design and performance evaluation of a laser based terrain-following controller for rotorcraft. The technique described achieves good terrain-following performance by taking into account, in the control law, the terrain characteristics ahead of the helicopter. Resorting to an $H_2$ controller design methodology for affine parameter-dependent systems, the technique presented exploits a new error space capable of naturally describing the particular dynamic characteristics of the helicopter in a suitable flight envelope. An alternative algorithm was proposed for computing the feedforward gain matrix that avoids solving linear matrix inequalities involving large numbers of unknowns. The resulting nonlinear controller was synthesized and implemented within the scope of gain-scheduling control theory, using a piecewise affine parameter-dependent model representation for the given set of operating regions. The effectiveness of the new control law was assessed in a MATLAB/Simulink simulation environment with a full nonlinear model of the Vario X-Treme helicopter. The quality of the results obtained clearly indicates that the methodology derived is suitable for the proposed application. Future work will include helicopter control close to the ground in the presence of strong wind action, extension of the presented technique to true three-dimensional terrain following using different sensors, and exploration of new error spaces along with new preview information inputs.

## Acknowledgments

This work was partially supported by Fundação para a Ciência e a Tecnologia (ISR/IST pluriannual funding) through the Programa Operacional Sociedade do Conhecimento that includes Fundo Europeu de Desenvolvimento Regional funds and by the POSI/SRI/41938/2001 ALTICOPTER project. The work of R. Cunha was supported by a Ph.D. student scholarship, SFRH/BD/5034/2001, from the Portuguese FCT Programa Operacional "Ciência, Tecnologia, Inovação."

## References

[1] Tomizuka, M., "Optimum Linear Preview Control with Application to

Vehicle Suspension—Revisited," *Journal of Dynamic Systems, Measurement, and Control*, Vol. 98, No. 3, 1976, pp. 309–315.
[2] Prokop, G., and Sharp, R. S., "Performance Enhancement of Limited Bandwith Active Automotive Suspensions by Road Preview," *Control Theory and Applications*, Vol. 142, No. 2, 1995, pp. 140–148.
[3] Takaba, K., "Robust Servomechanism with Preview Action for Polytopic Uncertain Systems," *International Journal of Robust and Nonlinear Control*, Vol. 10, No. 2, 2000, pp. 101–111.
[4] Hess, R. A., and Jung, Y. C., "An Application of Generalized Predictive Control to Rotorcraft Terrain-Following Flight," *IEEE Transactions on Systems, Man, and Cybernetics*, Vol. 19, No. 5, Sept. 1989, pp. 955–962.
[5] Ghaoui, L. E., and Niculescu, S. I., *Advances in Linear Matrix Inequality Methods in Control*, Society for Industrial and Applied Mathematics, SIAM, Philadelphia, PA, 1999.
[6] Boyd, S., Ghaoui, L. E., Feron, E., and Balakrishnan, V., *Linear Matrix Inequalities in Systems and Control Theory*, Society for Industrial and Applied Mathematics, SIAM, Philadelphia, PA, 1994.
[7] Cunha, R., and Silvestre, C., "A 3D Path-Following Velocity-Tracking Controller for Autonomous Vehicles," *Proceedings of the 16th IFAC World Congress*, Elsevier Science, Oxford, 2005.
[8] Silvestre, C., Pascoal, A., and Kaminer, I., "On the Design of Gain-Scheduled Trajectory Tracking Controllers," *International Journal of Robust and Nonlinear Control*, Vol. 12, No. 9, 2002, pp. 797–839.
[9] Kaminer, I., Pascoal, A., Hallberg, E., and Silvestre, C., "Trajectory Tracking for Autonomous Vehicles: An Integrated Approach to Guidance and Control," *Journal of Guidance, Control, and Dynamics*, Vol. 21, No. 1, 1998, pp. 29–38.
[10] Kaminer, I., Pascoal, A., Khargonekar, P., and Coleman, E., "A Velocity Algorithm for the Implementation of Gain-Scheduled Controllers," *Automatica: The Journal of IFAC, the International Federation of Automatic Control*, Vol. 31, No. 8, 1995, pp. 1185–1191.
[11] Cunha, R., and Silvestre, C., "Dynamic Modeling and Stability Analysis of Model-Scale Helicopters with Bell–Hiller Stabilizing Bar," *Proceedings of the AIAA Guidance, Navigation, and Control Conference*, AIAA, Reston, VA, 2003.
[12] Libório, G., Paulino, N., Cunha, R., Silvestre, C., and Ribeiro, M. I., "Terrain Following Preview Controller for Model-Scale Helicopters," *Proceedings of ICAR 2003—11th International Conference on Advanced Robotics*, Institute of Electrical and Electronics Engineers, Piscataway, NJ, 2003, pp. 1227–1232.
[13] Zhou, K., Doyle, J. C., and Glover, K., *Robust and Optimal Control*, Prentice–Hall, Inc., Upper Saddle River, NJ, 1995.
[14] Scherer, C., and Weiland, S., *Lecture Notes on Linear Matrix Inequalities in Control*, Dutch Institute of Systems and Control, Delft, The Netherlands, 2000.
[15] Rugh, W., and Shamma, J. S., "Research on Gain Scheduling," *Automatica*, Vol. 36, No. 10, 2000, pp. 1401–1425.